PNAS RESEARCH ARTICLE | EARTH, ATMOSPHERIC, AND PLANETARY SCIENCES OPEN ACCESS

Predicting nature-based coastal protection by mangroves under extreme waves

Zhan Hu[a,b,c], Stijn Temmerman[d], Qin Zhu[e,1], Xinran Wang[a], Jinwei Wu[a], Tianping Xu[a], Ken Schoutens[d], Tomohiro Suzuki[f], Zhifeng Yang[g], and Tjeerd J. Bouma[h,i]

Affiliations are included on p. 7.

Edited by Carlos Nobre, Universidade de Sao Paulo, Sao Jose dos Campos, Brazil; received May 31, 2024; accepted January 16, 2025

Forested wetlands such as mangroves are considered highly valuable for nature-based mitigation of coastal flooding. However, their wave attenuation capacity during extreme storms, when risks are highest, is rarely measured and remains challenging to predict. Here, we compile a unique dataset on the largest incident wave heights (0.39 to 1.44 m) ever recorded in forested wetlands, including our own measurements and literature data. Our analysis reveals that forested wetlands can significantly attenuate storm waves (35% over 3 wavelengths) except in rare near-submerged cases. Notably, 19 of the 20 existing formulations for vegetation drag coefficient, a key parameter for wave attenuation modeling, are inapplicable in storm conditions. Hence, we introduce an new approach to reliably predict wave attenuation during storms, without the need for drag coefficient determination nor modeling expertise. This approach offers coastal practitioners a new user-friendly tool to assess the effectiveness of nature-based solutions for storm hazard mitigation.

nature-based solutions | mangroves | coastal protection | extreme waves | wave modeling

Significance

We present evidence demonstrating that forested wetlands such as mangroves can sufficiently reduce record-high waves during storm events and thereby serve as a form of nature-based coastal protection. To reliably predict the protection capacity of forested wetlands, we employed a common modeling approach and 20 existing relations for vegetation drag coefficient, a critical parameter for wave attenuation modeling. Our results show that most of the exiting drag coefficient relations give acceptable predictions for small-wave cases, but their performance is poor in storm events. Therefore, we developed an new approach that predicts wave reduction by wetlands without the knowledge of drag coefficient nor modeling expertise. This approach is user-friendly and may serve as an important tool for managing nature-based coastal protection.

Wave attenuation by coastal and estuarine forested wetlands, such as mangrove and willow forests, is increasingly recognized as an important form of nature-based flood risk mitigation (1–3). Global-scale numerical modeling shows that mangrove forests can sufficiently attenuate storm waves, thereby reducing wave run-up and wave overtopping on sea walls (4). This could lower the height of sea walls, potentially saving up to 100 billion USD in global coastal protection costs (5). Regional remote sensing studies also confirm the protective role of forested wetlands (6, 7), especially in rural coastal communities lacking coastal protection infrastructure (8).

Beyond large-scale assessments, in situ measurements of wave attenuation in forested wetlands during extreme storm events are relatively rare and only available for case-specific locations (9), while measurements for cases of small or moderate incident waves are more widely available. This is likely due to restricted accessibility of forested wetlands during storms when they are deeply inundated and subject to strong waves. Hence, relatively few case studies show empirical evidence on how much protection coastal forested wetlands can provide during the extreme storm events (7, 10), when protection is most needed. Consequently, as such empirical data is lacking for many locations, obtaining reliable prediction of wave damping during extreme storms is a necessity for coastal managers to design and implement nature-based coastal protection on a large-scale.

Various complex numerical models have been developed to assess wave damping by coastal forested wetlands (11). However, these models are often inaccessible to coastal managers, consultants, and scientists, who typically lack advanced modeling expertise. Additionally, there is a common challenge across all existing models regardless of complexity: determining the vegetation drag coefficient (C_D) (9). This dimensionless coefficient (0.1 to 100) accounts for the drag of forest stems to the wave motion (12), which varies with both hydrodynamic conditions (e.g., flow velocity and turbulence) and vegetation characteristics (e.g., density and flexibility). Many empirical relations have been proposed to determine C_D (13, 14), but their applicability in storm events is still unclear. This poses a major uncertainty in evaluating and implementing coastal forested wetlands for nature-based coastal protection.

In this study, we compiled a unique dataset of the top 50 highest incident significant wave heights (H_{s0}) recorded in coastal and estuarine forested wetlands, i.e., mangroves and willows. The significant wave height (H_s), a widely used statistic to summarize a recorded wave height spectrum, is the average of the 1/3 highest waves observed at a place over typically 15 to 30 min. This dataset includes our own in situ measurements of a storm event in August 2022 on Hailing Island, China, as well as data from previous laboratory

Author contributions: Z.H., S.T., Q.Z., K.S., Z.Y., and T.J.B. designed research; Z.H., S.T., Q.Z., X.W., T.X., T.S., Z.Y., K.S., T.S., and T.J.B. performed research; Z.H., S.T., Q.Z., J.W., T.X., K.S., T.S., and T.J.B. contributed new reagents/analytic tools; Z.H., Q.Z., X.W., J.W., T.X., K.S., and T.S. analyzed data; and Z.H., S.T., Q.Z., X.W., J.W., T.X., K.S., T.S., Z.Y., and T.J.B. wrote the paper.

The authors declare no competing interest.

This article is a PNAS Direct Submission.

Copyright © 2025 the Author(s). Published by PNAS. This open access article is distributed under Creative Commons Attribution-NonCommercial-NoDerivatives License 4.0 (CC BY-NC-ND).

[1]To whom correspondence may be addressed. Email: zhuqin@gmlab.ac.cn.

This article contains supporting information online at https://www.pnas.org/lookup/suppl/doi:10.1073/pnas.2410883122/-/DCSupplemental.

Published March 17, 2025.

Downloaded from https://www.pnas.org by 84.17.46.190 on April 30, 2025 from IP address 84.17.46.190.

and field observations whose H_{s0} reached top 50. These observations are from Delta flume, the Netherlands (15), Cù Lao Dung Island, Vietnam (16), and Shanwei coast, China (17). We used this synthesis of top 50 H_{s0} ($H_{s0} \geq 0.39$ m) wave data to 1) demonstrate the wave damping capacity of coastal forested wetlands under extreme storm wave conditions; 2) evaluate the applicability of 20 existing C_D formulations in storm wave conditions; 3) develop an new easy-to-use empirical method to predict wave damping by coastal forested wetlands without the need of preknowledge on C_D nor quantification of the forest characteristics. This new method is called *HU* method, as it is based on H_{Ln}–Ur relations, via which relative wave height at nth wavelength into the wetland canopy (H_{Ln}) can be derived for a given *Ursell* number (Ur).

Results

Top 50 Cases of Incident Wave Height at Coastal Forest Edge. In 2022, typhoon Chaba and Ma-on brought strong wind and high waves to a large part of the south China coast (18) (Fig. 1*A*). On Hailing Island, our wave measuring transect recorded the extreme high waves propagating from bare tidal flat into a mature mangrove forest (Fig. 1*B*). The incident significant wave height (H_{s0}) recorded at the seaward mangrove edge reached 0.72 m with water depth greater than 2 m (Fig. 1*C*). To our knowledge, this is one of the highest H_s values ever measured in natural mangroves (Table 1 and *SI Appendix*, Table S1). A boardwalk for tourists was severely damaged during Typhoon Chaba at our observation site, showing the tremendous force of the incident waves (Fig. 1*D*). Notably, during both typhoons, H_{s0} were sufficiently attenuated by 73 to 86% over the 216 m long mangrove measuring sections (Fig. 1*B*). The attenuation of waves can be observed from the photos taken at the pioneer zone and mature forest during a windy day (Fig. 1 *E* and *F*). The mean canopy height of the mature forest is 2.6 m, which is dominated by native *Avicennia marina* and occasional *Kandelia obovate* and exotic *Sonneratia apetala* trees.

Combining the above-mentioned own measurements and literature data, we compiled a unique dataset of the top 50 H_{s0} values measured at the edge of mangroves or estuarine wetlands canopies (Table 1). This dataset is obtained by reviewing and ranking the existing studies with wave measurements in coastal and estuarine forested wetlands (Fig. 2 and *SI Appendix*, Table S1). We find that our own measurements together with measurements from Mekong

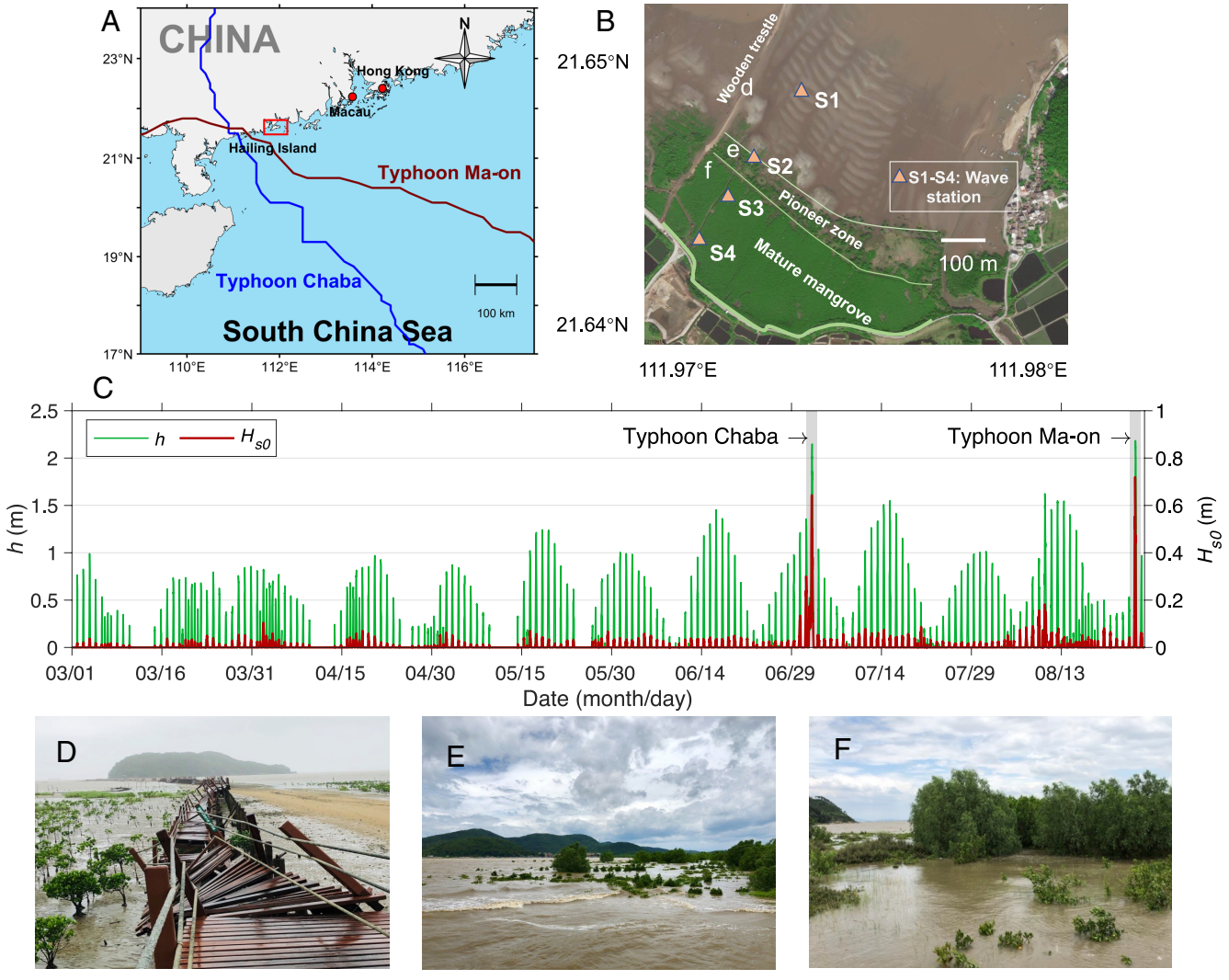

Fig. 1. (*A*) Field site location (Hailing Island, south China) and the tracks of Typhoon Chaba and Ma-on. (*B*) Deployment of four wave sensors at the field site on Hailing Island. Measuring station S1 was positioned on the bare tidal flat, S2 at the edge between the bare tidal flat and the pioneer mangroves, S3 and S4 within the landward mature mangroves. The letters "d," "e," and "f" indicate the locations of photographs in panels (*D*–*F*). (*C*) Measured significant incident wave height (H_{s0}) and water depth (h) at seaward mangrove edge (station S2). (*D*) Destroyed boardwalk at the study site after Typhoon Chaba. (*E* and *F*) Photographs of pioneer zone and mature forest under high water depth.

Downloaded from https://www.pnas.org by 84.17.46.190 on April 30, 2025 from IP address 84.17.46.190.

Delta of Vietnam (16), Shanwei Coast in China (17), as well as a wave flume experiment in Delft, the Netherlands (15), have recorded the highest 50 H_{s0}, ranging from 0.39 m to 1.44 m. By contrast, more than 70% of the reviewed studies have recorded smaller H_{s0} values, ranging from 0.11 m to 0.35 m (Fig. 2 and *SI Appendix*, Table S1).

The compiled dataset shows that forested wetlands can significantly reduce wave height during storms. H_{s0} is reduced by 2 to 38% over the first wavelength, and 42 to 75% over five wavelengths, provided the forest canopy is long enough (Table 1). It takes 33 to 90 m of forested wetlands to halve the H_{s0} (*SI Appendix*, Table S2). Thus, 100 m can be a sensible minimum width when designing forested wetlands for storm wave protection, where the storm water depth is approximately less than 50% of the canopy height. Notably, waves were barely damped (only 2 to 3%) over the pollard willow trees in the Delta flume experiments (case D1 to D4 in *SI Appendix*, Table S2), when tested with the highest H_{s0} (1.4 m) and water depth (4.5 m). In these cases, trees were nearly submerged and branches start to sway possibly due to the strong overturning moment acting on the tree branches (15, 30).

Evaluating the Applicability of 20 Existing C_D Relations. We embedded 20 different C_D relations (*SI Appendix*, Table S3) in an advanced wave transformation model (SWASH) (11) to determine C_D values and simulate the consequential wave height reduction in both top 50 H_{s0} cases and small H_{s0} cases (see *Methods* and *SI Appendix*, Table S2 for the tested cases). The modeled wave height reduction was compared against the measured data in the corresponding cases to assess the applicability of existing C_D relations in different wave conditions. An example of the top 50 H_{s0} cases (from our measurement) shows that different C_D relations led to various degrees of wave damping predictions (Fig. 3*A*). In this example, the predicted H_s reduction ranges from 0.14 to 0.70 m over a cross-shore distance of 216 m, while the measured H_s reduction was 0.59 m between station S2 and S4.

The tested C_D relations generally perform better in low H_{s0} cases comparing to high H_{s0} cases. As an example, modeling outcomes generated by C_D relation 7 are in reasonable agreement with relatively small H_{s0} cases (<0.72 m), but for cases with higher H_{s0} (≥0.72), the deviation from the measured data is apparent (Fig. 3*B* and *SI Appendix*, Fig. S1 for all relations). To fully reveal the applicability of these C_D relations, we apply them in three collections of H_{s0}: top 10, top 50 and small H_{s0} (H_{s0} < 0.2 m, *SI Appendix*, Table S2). For 9 out of 20 C_D relations, R^2 is high for small incident wave cases (R^2 value > 0.6) but much less in top 50 and top 10 H_{s0} cases (Group 2 in Fig. 3*C*). Additionally, another 9 C_D relations were neither good in simulating small nor large wave cases (i.e., R^2 value < 0.6, Group 3 in Fig. 3*C*). These results imply that if the tested C_D relations are originally derived from low incident wave cases, they are generally not applicable for high incident wave cases such as during tropical cyclones. Among all C_D relations, relation 1 (31) $C_D = 70{*}KC^{-0.86}$ is an exception, whose performance for both large and small incident waves is fairly good, even for top 10 H_{s0} cases (i.e., R^2 values all above 0.6).

A New User-Friendly Approach to Assess Wave Damping in Forested Wetlands. Since there is large uncertainty in determining C_D values to assess wave damping in extreme cases, we developed an approach to assess wave damping in coastal forested wetlands without preknowledge of C_D nor expertise in modeling. This approach is called the *HU* method, since it is based on the relations between the relative wave height at *n*th wavelengths in canopy (H_{Ln}) and the *Ursell* number (*Ur*). H_{Ln} is defined as H_{sn}/H_{s0}, where H_{sn} is the H_s after the wave has traveled over *n* wavelengths into the vegetation canopy As an index of wave nonlinearity, *Ur* is defined as $H_{s0}\,L^2/D^3$, where *L* is wavelength and *D* is water depth at the seaward edge of the canopy (32–34).

We show that at integral multiple of wavelength (e.g., n = 1, 5, 10), H_{Ln} decreases with increasing *Ur* number (Fig. 4*A*), regardless of low (<0.39 m) or high H_{s0} (≥0.39 m). At each wavelength, a general form of the H_{Ln}–*Ur* relation can be derived based on the observed data of low H_{s0} cases

$$H_{Ln} = 1/\left(1 + a^{*}Ur^{b}\right), \quad [1]$$

where a = [0.05 to 0.6] and b = [0.42 to 0.57] are calibration parameters that vary at each multiple of wavelength. Since *Ur* is proportional to D^{-3}, small H_{s0} cases that are associated with shallow water can have similar magnitude of *Ur* as high H_{s0} cases. This property enables the acquisition of the H_{Ln}–*Ur* relations from frequently occurring small H_{s0} cases. Our analysis shows that the H_{Ln}–*Ur* relations derived from small H_{s0} cases fit well with the data in large H_{s0} cases (Fig. 4*A*).

The assembly of the derived H_{Ln}–*Ur* relations at each multiple of wavelength through the canopy (i.e., n = 1, 2, ...) provide a new pathway (i.e., *HU* method) to predict wave attenuation (Fig. 4*A*). For a given *Ur*, H_{Ln} along a forested wetland can be derived via each H_{Ln}–*Ur* relation. For instance, if *Ur* = 30, the

Table 1. Top 50 incident significant wave heights (H_{s0}) ever recorded in coastal and estuarine forested wetlands

Source	Incident significant wave height (H_{s0}) (m)	Water depth (m)/canopy height (m)	Peak Wave period (s)	Dominant plant species	Number of cases in top 50/ top 10 H_{s0} list	H_s damping (%) over 1, 5 wavelength
Delta flume, Delft, the Netherlands (15)	0.44 to 1.44	3, 4.5/5.5	2.8 to 6.9	Willow (*Salix alba*)	12/8	2 to 24, —
Hailing Island, China (this study)	0.39 to 0.72	1.1 to 2.3/2.6	3.9 to 5.8	Mangrove (*A. marina*)	33/1	13 to 26, 42 to 64
Cù Lao Dung Island, Mekong Delta, Vietnam (16)	0.42 to 0.72	0.9 to 1.4/2.0 to 18.0	3.8 to 3.9	Mangrove (*Sonneratia caseolaris*, *Sonneratia alba*)	4/1	13 to 19, 44 to 54
Shanwei coast, China (17)	0.40	1.3/3.0 to 4.0	5.0 to 6.1	Mangrove (*Laguncularia racemosa*)	1/0	38, 75

Downloaded from https://www.pnas.org by 84.17.46.190 on April 30, 2025 from IP address 84.17.46.190.

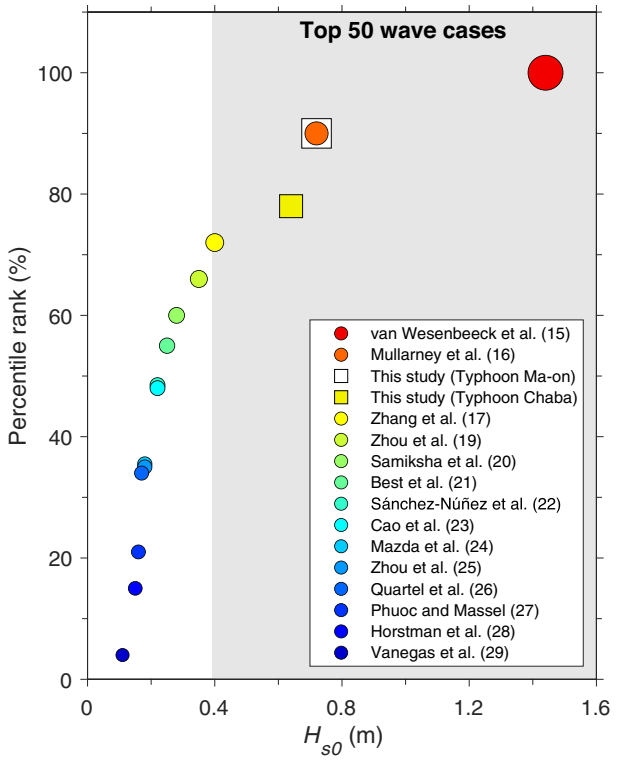

Fig. 2. Percentile ranking of incident significant wave heights (H_{s0}) measured at the edge of forested wetlands, compiled from literature (15–17, 19–29) and our measured dataset. The gray area indicates studies with top 50 H_{s0} data (H_{s0} > 0.39 m), ranked above ca. 70% of all studies. All the data are from field measurements in mangrove forests, except for Van Wesenbeeck et al. (15), which is a laboratory flume experiment with willow trees, i.e., estuarine forested wetland vegetation (see *SI Appendix*, Table S1 for the full list).

relative wave height decreases from H_{L1} = 0.81 to H_{L2} = 0.67 and further decreases to H_{L15} = 0.19 (Fig. 4*B*). Notably, since H_{Ln} is a relative wave height, its reduction rate in space is the same for different absolute H_{s0}. The newly developed *HU* method for wave attenuation assessment can be divided into two steps: first, derive empirical H_{Ln}–*Ur* relations at each multiple of wavelength based on measured data of frequently occurring small H_{s0} cases (Fig. 4*A*); second, for a given *Ur*, the reduction trend of H_{Ln} through the forested wetland can be obtained and applied to predict wave attenuation in rare (nonmeasured) high H_{s0} cases (Fig. 4*B*).

To test the applicability of the new *HU* method, it is applied to assess wave attenuation in the top 50 H_{s0} cases and additional field data from Beibu Bay, South China (Fig. 4*C*, $H_{s0} \leq 0.35$) (19). These additional data were included to test the applicability of this method in submerged mangrove canopies. At each site of the top 50 H_{s0} cases, a set of H_{Ln}–*Ur* relations were built based on the local small H_{s0} cases (H_{s0} = 0.05 to 0.4 m, *SI Appendix*, Table S4) and was subsequently applied to predict wave dissipation in storm-like high H_{s0} cases (*SI Appendix*, Table S4).

The overall accuracy of this approach is high (R^2 = 0.77, Fig. 4*C*). The RMSE for H_{Ln} ranges from 0.04 to 0.08 for all tested cases (*SI Appendix*, Table S4). The RMSE for the additional site (Beibu Bay) is higher (0.16) compared to other sites, likely caused by the submergence of the young (<5 y) and short forest canopy there (19). The submerged canopy provides less drag to the water column, and thus lower dissipation as estimated by the *HU* method. Results from Beibu Bay indicate an application limit of this new method. If the submerged canopy data from the Beibu Bay area are excluded, the accuracy of this approach can be much improved with R^2 value being 0.92, which is much higher than the conventional method relies on C_D parametrization.

Discussion

Nature-based coastal risk mitigation by forested wetlands such as mangroves is highly valued, yet empirical evidence and predictive capacity of wave attenuation by forested wetlands are very limited during extreme wave conditions, when coastal flooding risk is most critical. Here, we present a unique dataset of the top 50 incident wave height recorded in coastal forested wetlands including newly collected typhoon measurements. This dataset shows that coastal forested wetlands can effectively damp waves even during high-energy conditions, with H_s reduction exceeding 40% over five wavelengths (Table 1). Under the most extreme waves in this dataset (D1 to D4 in *SI Appendix*, Table S2), swaying of the flexible pollard-willow-branches leads to sharp reduction in wave damping (15), but such reduction is not observed in other top 50 H_{s0} cases from mangrove forests (Table 1 and *SI Appendix*, Table S2). Vegetation swaying under extreme waves is likely a self-protection mechanism to avoid drag overloading and stem breakage (35, 36). Further study is needed on the tipping point where trees start to sway and determine the critical wave damping capacities.

The top 50 H_{s0} dataset provides a key opportunity to test the applicability of existing C_D relations in predicting wave damping. We find that 19 out of 20 tested empirical relations fail to yield suitable drag coefficients in extreme wave conditions. The reason is likely that most of these C_D relations are derived from nonextreme, mild conditions. Thus, their application range is confined to these conditions and may not be extended to extreme wave cases. Differences in horizontal and vertical flow structures across wave conditions may contribute to this limitation. Horizontally, high waves generate elevated orbital motion, engaging more vegetation stems in flow interaction. This leads to constricted flow between stems and reduced wake pressure behind stems, known as blockage effects (37). In low wave conditions, reduced wave motion minimizes blockage effects on C_D, bringing it closer to values for a single cylinder in oscillatory flow. In the vertical direction, the velocity structures tend to be uniform in shallow water depths that sustain low incident waves (38). However, high wave cases occur with much larger water depths, in which the vertical velocity variation is apparent with higher velocity near the water surface. Thus, the different velocity structures would lead to different drag forms and C_D parametrization, which should be accounted for.

Notably, the exceptional C_D relation that provides reliable wave estimation (R^2 > 0.8) was derived from a storm event (31) (i.e., relation 1 in *SI Appendix*, Table S3, a C_D-KC relation). This relation was derived from a *Spartina* marsh with a high solid volume fraction of 0.02 ($\phi = N\pi d^2/4$, N and d are stem density and diameter, respectively). This ϕ is comparable to the mangrove forest at our field site (0.006), considering the large variability of mangrove canopy geometry (ϕ = 0 to 0.45). The similar volume fractions and hydrodynamic conditions (storm waves) may lead to the good performance of this C_D relation at our site. However, another C_D relation (i.e., relation 14), which was also derived based on the same stormy data but in a different form (31), has much poorer model performance (R^2 < 0.1). This indicates that C_D relation should be selected cautiously, and the relations derived from extreme wave cases at certain sites may not be applied elsewhere.

Given the uncertainty in $C_D$estimation, we developed the new *HU* method for wave attenuation assessment during storm events. This method, based on H_{Ln}–*Ur* relations (Eq. **1**), leverages the

Downloaded from https://www.pnas.org by 84.17.46.190 on April 30, 2025 from IP address 84.17.46.190.

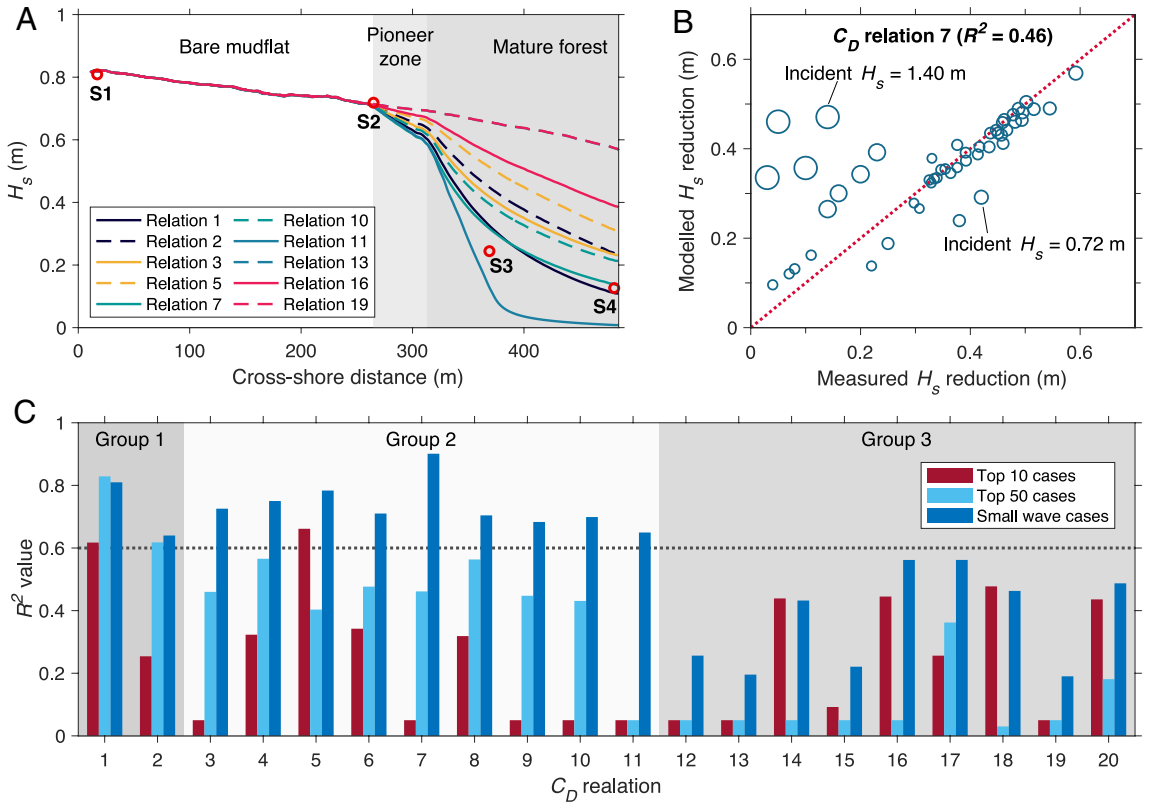

Fig. 3. (*A*) Modeling results of one case in the top 50 H_{s0} datasets (from our observations) compared with measurements. Red circles indicate measurements from station S1 to S4 at our study site on Hailing Island. Bathymetry of the measurement transect is incorporated in the modeling. For visualization purpose, only 10 (out of 20) modeled *Hs* results from different C_D relations are plotted to avoid overlaps between different lines. (*B*) Example of applying C_D relation 7 embedded in SWASH to model the cases of top 50 H_{s0}. This relation is chosen for its moderate performance (R^2 = 0.46), representing the average performance level of all 20 relations. Model performances for all the 20 C_D relations are listed in *SI Appendix*, Fig. S1. The size of the data points indicates H_{s0} value. (*C*) overall model performance with all 20 C_D relations for top 10, top 50, and small H_{s0} cases. Based on model performance, these relations can be divided into three groups: Group 1 (relation 1 and 2) has high R^2 values (>0.6) for both top 50 and small H_{s0} cases; Group 2 (relation 3 to 11) has high R^2 values only for small H_{s0} cases; Group 3 (relation 12 to 20) does not have high R^2 values for any H_{s0} cases. The top 10 H_{s0} cases are included to show model performances in extreme high wave conditions ($H_{s0} \geq 0.72$). For visualization, R^2 values below zero are assigned a constant value of 0.05.

increase in orbital velocity skewness with higher *Ur* (*SI Appendix*, Fig. S7). An increase in *Ur* would elevate peak velocities and enhance overall wave energy dissipation (Fig. 4*A* and *SI Appendix*, Fig. S6). Since *Ur* (as an index for wave nonlinearity) varies greatly with water depth and wave period, even small H_{s0} cases can exhibit a wide range of *Ur*, hence including storm wave cases as well. Consequently, H_{Ln}–*Ur* relations derived from common low H_{s0} cases enable the assessment of rare storm wave H_{Ln} evolution along the wavelength. A detailed illustration on the mechanism of the *HU* method is included in *SI Appendix*, Text S1.

This new method marks an advancement with three primary advantages: 1) it eliminates the need for C_D values and canopy characteristics (e.g., stem density, diameter) of natural forested wetlands in assessment. This is a key advancement, as both types of parameters can vary greatly and are typically very difficult to determine in the field. Although a C_D-free method exists for marsh vegetation (39), canopy height and standing biomass are still necessary for assessment. 2) Since this new method relies on H_{Ln}–*Ur* relations, and high wave cases may have similar *Ur* ranges as small wave cases with similar nonlinearity (Fig. 4*A*), this approach can be applied as a bridge to assess wave damping in extreme wave conditions based on more assessable data of small or moderate waves. 3) This approach does not require expertise in numerical modeling, offering a user-friendly tool for local coastal managers and scientists to assess the wave damping capacity of coastal forested wetlands. A detailed instruction of applying the *HU* method is provided in Text S1.

Yet, this approach has certain limitations: 1) As H_{Ln}–*Ur* relations are derived from local measurements, this approach is expected to be site-specific, requiring recalibration if forest canopy structure changes over time. 2) This approach may only be applicable to rigid and emergent coastal forested wetlands, such as mature mangroves, as submergence or swaying of the canopy can lead to significant reduction of the wave dissipation (e.g., data from Beibu Bay in Fig. 4*C* as a submerged example).

Through analysis of the 50 highest recorded incident waves, this study demonstrates the wave damping capacity of coastal forested wetlands during storm events, exhibiting a positive outlook to restore forested wetlands for coastal protection (40) alongside many other ecosystem services. Furthermore, the developed *HU* method provides a new avenue to predict wave damping capacity of forested wetlands during extreme storms. To make it work, it only requires in situ wave measurements by a transect of pressure sensors over, e.g., a spring-neap tidal cycle during the windy season, but without need for inclusion of extreme storms. This is doable at many locations across the globe, especially if governmental organizations or NGOs would provide a single set of pressure sensors to be used for sequential measuring campaigns across the country. As such, the newly introduced *HU* method offers an easy-to-use tool for coastal practitioners to assess wave attenuation capacity of forested wetlands during storm events and to plan for implementation of nature-based coastal hazard mitigation schemes.

Downloaded from https://www.pnas.org by 84.17.46.190 on April 30, 2025 from IP address 84.17.46.190.

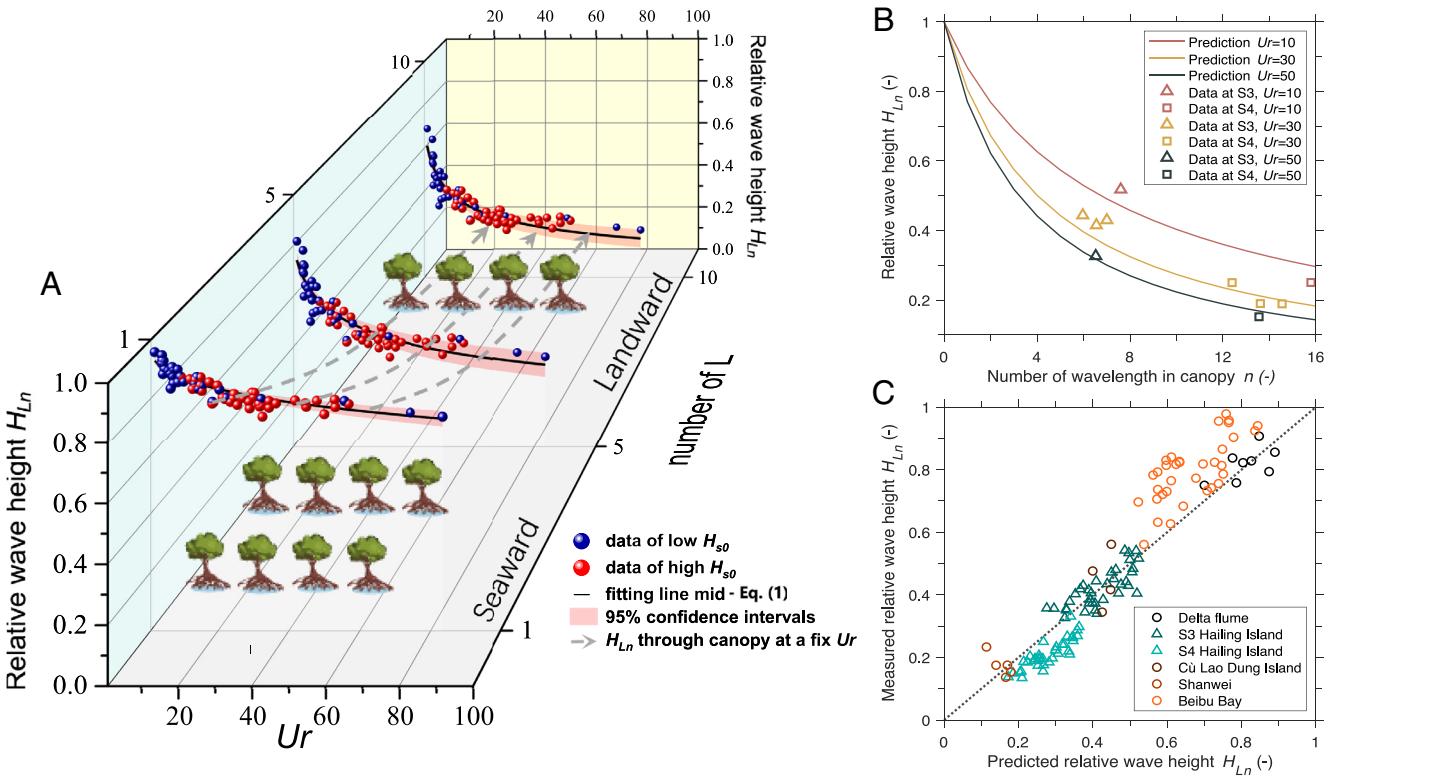

Fig. 4. (*A*) Relative wave height (H_{Ln}) after the waves travel 1, 5, and 10 wavelengths (*L*) through the mangrove canopy with both low incident wave (H_{s0} < 0.39) and high incident waves (H_{s0} ≥ 0.39) at Hailing Island site. Data points are obtained by extrapolating the measured relative wave height (*SI Appendix*, Eq. **S4**). The fitted lines are H_{L1}–*Ur*, H_{L5}–*Ur*, and H_{L10}–*Ur* relations derived using only low H_{s0} data. The dashed arrow lines indicate the reduction of H_{Ln} through the canopy at a fixed *Ur*, illustrating the core concept of *HU* method. (*B*) Predicted H_{Ln} values compared to the measurements from stations S3 and S4 on Hailing Island when *Ur* = 10, 30 and 50. The data points are from high H_{s0} cases (H_{s0} ≥ 0.39), while the predictions are derived based on H_{Ln}–*Ur* relations of low H_{s0} cases. (*C*) Comparison between predicted and measured H_{Ln} values in the top 50 H_{s0} cases and additional measurements with submerged mangrove canopies from Beibu Bay, China (19). At each site, predictions for high H_{s0} cases are made based on low H_{s0} data from the local measurement (see *SI Appendix*, Table S4 for details). The overall prediction R^2 is 0.77, increasing to 0.92 if data from submerged canopies are excluded.

Methods

Observations of Hydrodynamics and Canopy Characteristics. At our study site on Hailing Island, China, wave data were collected using pressure sensors (RBRsolo^3). Along a transect from bare tidal flat into pioneer zone and further into mature mangrove forest, four sensors were deployed from March 2022 to September 2022 (41). The sampling frequency was set at 4 Hz, and the interval was set at 10 min. In one interval, 4,096 bursts of pressure data were collected. Significant wave height, peak wave period, and water depth were obtained following a standard calculation method (41, 42).

The mature mangrove forest is dominated by native *A. marina* with a few *K. obovate* and exotic *S. apetala* trees growing in the seaward fringe (Fig. 1). A vegetation survey was conducted during July 2022. We sampled 12 *A. marina* and 6 *K. obovate* trees in total. The height of the trees was measured by a leveling rod (*SI Appendix*, Fig. S2). The mean height for *A. marina* and *K. obovate* is 2.6 m and 0.9 m, respectively. The morphology of the trees was measured following the method of Zhang et al. (17) The diameter of the stem was measured near the 1st order of branch. The vertical distribution of frontal area that is relevant for wave damping was obtained by multiplying the averaged frontal area of each tree and the number of trees per unit area (*SI Appendix*, Fig. S2). At our measuring site, no uprooting or deadly stem breakage was found after typhoon Chaba and Ma-on, similar to the other measurements in the top 50 H_{s0} cases.

Compiling Data of Top 50 Incident Wave Height. We compiled data from literature on the top 50 H_{s0} values measured in studies on wave attenuation by coastal or estuarine forested wetlands. The dataset consists of the Delta flume experiment, and three field measurements, including our field-measured data (Table 1). The Delta flume experiment tested wave damping by willow trees (estuarine wetlands species) in a 300 m long wave flume (15). In this experiment, H_{s0} as high as 1.44 m was recorded, which is the highest H_{s0} recorded for forested wetland vegetation (Fig. 2). The observation in the Mekong Delta was conducted in 2015, in which the highest H_{s0} at the mangrove edge was 0.72 m (16). The observations at the Shanwei coast captured wave propagation in a mangrove forest during the Mangkhut typhoon (2018) (17). A maximum 0.40 m H_{s0} was recorded during this event.

Wave Modeling and Equations. We developed the *HU* method to predict wave damping capacity during storm conditions. This method is based on the wave measurements in the wetland canopy and subsequent data processing procedures based on H_{Ln}–*Ur* relations. The form of H_{Ln}–*Ur* relation is given as Eq. **1**, via which relative wave height along the canopy (H_{Ln}) can be derived at a given *Ur* number. H_{Ln} is defined as H_{sn}/H_{s0}, where H_{s0} is the incident H_s and H_{sn} is the H_s at *nth* multiple of wavelength into the vegetation canopy. A detailed workflow and data processing files of the *HU* method are given in Text S1.

To test the existing C_D relations, we embedded them in an open-source numerical hydrodynamic model (SWASH, Simulating Waves till Shore) (11, 43) to simulate the wave height evaluation in both top 50 H_{s0} cases and the small H_{s0} cases (see *SI Appendix*, Table S2 for the list of the tested cases). Subsequently, the modeling results of wave dissipation were compared against the measurements as an evaluation of the C_D relations. Additionally, we applied the SWASH model to explain the mechanism of H_{Ln}–*Ur* relations (*SI Appendix*, Text S1). We chose the SWASH model for such purpose as the governing equations of the model are nonlinear shallow water equations, from which the orbital velocity and the nonlinear wave attenuation process can be assessed.

Coastal forests were modeled as rigid emergent cylinders (11, 37). The vegetation drag force is assessed following the Morison equation (44) and included in the momentum equation:

$$F_D = \frac{1}{2}\rho C_D h_v N d u(t)|u(t)|, \qquad [2]$$

Downloaded from https://www.pnas.org by 84.17.46.190 on April 30, 2025 from IP address 84.17.46.190.

where ρ is the water density, h_v is the vegetation height in the water column, N is the number of stems per square meter, d is stem diameter, and $u(t)$ is the wave orbital velocity in time. Since C_D needs to be determined prior to the SWASH modeling, we use an approximation method to obtain the C_D values based on the existing C_D relations (*SI Appendix*, Table S3). We first assume a spatially constant C_D value of 2 to acquire a preliminary assessment of wave height and orbital velocity. Subsequently, the obtained spatially varying orbital velocity values were used to obtain Reynolds numbers (Re) and Keulegan–Carpenter numbers (*KC*) (Eqs. **3** and **4**). Then, the *Re* or *KC* numbers were applied in C_D relations to obtain another series of spatially varying C_D, which will be used in the next run of SWASH modeling. This loop is terminated until the maximum difference between the freshly derived series of C_D and the previous series is less than 10%. The wave height results of the last run were then used as the outcome of wave attenuation assessment of a C_D relation. For most cases, it takes 3 to 6 runs till the loop is ended. *Re* number is defined as

$$Re = \frac{|u_{max}|d}{\nu}, \quad [3]$$

where u_{max} is orbital wave velocity with the maximum amplitude, d is the mean diameter of the vegetation stems, and ν is kinematic viscosity of water. *KC* number is defined as

$$KC = \frac{|u_{max}|T_p}{d}, \quad [4]$$

where T_p is the peak wave period.

Data, Materials, and Software Availability. All study data are included in the article and/or *SI Appendix*. The DOI of the code and exemplify datasets is available via the following link: https://data.4tu.nl/private_datasets/0UhrjZSgf1MuwyGITA-3N3yCBm3-Ngz7Xr6ajcHSrnI (45).

ACKNOWLEDGMENTS. We would like to thank the members of M5 Lab (Mudflat, Marsh, Mangrove, Measurement & Modeling) at Sun Yat-sen University and Hailing Island Mangrove National Wetland Park for their support in the field work. This work is supported by Guangdong Provincial Department of Science and Technology (2024B1515020066), the National Natural Science Foundation of China (52388101, 42176202, 52239005, and 52471287), Guangdong Provincial Department of Science and Technology (2019ZT08G090 and 2019ZT08L213), Innovation Group Project of Southern Marine Science and Engineering Guangdong Laboratory (Zhuhai) (311021004), 111 Project (B21018).

Author affiliations: [a]School of Marine Sciences, Sun Yat-Sen University and Southern Marine Science and Engineering Guangdong Laboratory (Zhuhai), Zhuhai 519082, China; [b]State Key Laboratory of Environmental Adaptability for Industrial Products, Sun Yat-Sen University, Zhuhai 519082, China; [c]Guangdong Provincial Key Laboratory of Marine Resources and Coastal Engineering, Zhuhai 519082, China; [d]Ecosphere Research Group, University of Antwerp, Antwerp 2020, Belgium; [e]Guangdong Basic Research Center of Excellence for Ecological Security and Green Development, Southern Marine Science and Engineering Guangdong Laboratory (Guangzhou), Guangzhou 511458, China; [f]Department of Civil Engineering, Katholieke Universiteit Leuven, Leuven 3001, Belgium; [g]School of Ecology, Environment and Resources, Guangdong University of Technology, Guangzhou 510006, China; [h]Department of Estuarine and Delta Systems, the Royal Netherlands Institute for Sea Research (NIOZ), Utrecht University, Yerseke 4401 NT, The Netherlands; and [i]Department of Physical Geography, Faculty of Geosciences, Utrecht University, Utrecht 3584 CB, The Netherlands

1. S. Temmerman *et al.*, Ecosystem-based coastal defence in the face of global change. *Nature* **504**, 79–83 (2013).
2. C. Duarte, I. J. Losada, I. Hendriks, I. Mazarrasa, N. Marba, The role of coastal plant communities for climate change mitigation and adaptation. *Nat. Clim. Change* **3**, 961–968 (2013).
3. Z. Zhu *et al.*, Historic storms and the hidden value of coastal wetlands for nature-based flood defence. *Nat. Sustainability* **3**, 853–862 (2020), 10.1038/s41893-020-0556-z.
4. R. Van Coppenolle, C. Schwarz, S. Temmerman, Contribution of mangroves and salt marshes to nature-based mitigation of coastal flood risks in major deltas of the world. *Estuaries Coasts* **41**, 1699–1711 (2018).
5. V. T. M. van Zelst *et al.*, Cutting the costs of coastal protection by integrating vegetation in flood defences. *Nat. Commun.* **12**, 6533 (2021).
6. S. Das, J. R. Vincent, Mangroves protected villages and reduced death toll during Indian super cyclone. *Proc. Natl. Acad. Sci. U.S.A.* **106**, 7357–7360 (2009).
7. J. P. Hochard, S. Hamilton, E. B. Barbier, Mangroves shelter coastal economic activity from cyclones. *Proc. Natl. Acad. Sci. U.S.A.* **116**, 12232–12237 (2019).
8. C. E. J. van Bijsterveldt *et al.*, Subsidence reveals potential impacts of future sea level rise on inhabited mangrove coasts. *Nat. Sustainability* **6**, 1565–1577 (2023), 10.1038/s41893-023-01226-1.
9. S. Temmerman *et al.*, Marshes and mangroves as nature-based coastal storm buffers. *Annu. Rev. Mar. Sci.* **15**, 95–118 (2023).
10. A. H. Baird, R. S. Bhalla, A. M. Kerr, N. W. Pelkey, V. Srinivas, Do mangroves provide an effective barrier to storm surges? *Proc. Natl. Acad. Sci. U.S.A.* **106**, E111–E111 (2009).
11. T. Suzuki, Z. Hu, K. Kumada, L. K. Phan, M. Zijlema, Non-hydrostatic modeling of drag, inertia and porous effects in wave propagation over dense vegetation fields. *Coast. Eng.* **149**, 49–64 (2019).
12. H. M. Nepf, "Flow over and through biota" in *Treatise on Estuarine and Coastal Science*, E. Wolanski, D. McLusky, Eds. (Academic Press, 2011), pp. 267–288.
13. H. Chen *et al.*, Deriving vegetation drag coefficients in combined wave-current flows by calibration and direct measurement methods. *Adv. Water Res.* **122**, 217–227 (2018).
14. L. Zhu *et al.*, Towards a unified drag coefficient formula for quantifying wave energy reduction by salt marshes. *Coastal Eng.* **180**, 104256 (2023).
15. B. K. van Wesenbeeck *et al.*, Wave attenuation through forests under extreme conditions. *Sci. Rep.* **12**, 1884 (2022).
16. J. C. Mullarney, S. M. Henderson, J. A. H. Reyns, B. K. Norris, K. R. Bryan, Spatially varying drag within a wave-exposed mangrove forest and on the adjacent tidal flat. *Cont. Shelf Res.* **147**, 102–113 (2017).
17. X. Zhang, P. Lin, X. Chen, Coastal protection by planted mangrove forest during typhoon Mangkhut. *J. Mar. Sci. Eng.* **10**, 1288 (2022).
18. C. Chen *et al.*, Tracks of typhoon movement (left and right sides) control marine dynamics and eco-environment in the coastal bays after typhoons: A case study in Zhanjiang Bay. *Sci. Total Environ.* **912**, 168944 (2024).
19. X. Zhou *et al.*, Linkage between mangrove wetland dynamics and wave attenuation during a storm–A case study of the Nanliu Delta, China. *Mar. Geol.* **454**, 106946 (2022).
20. S. V. Samiksha *et al.*, Attenuation of wave energy due to mangrove vegetation off Mumbai, India. *Energies* **12**, 4286 (2019).
21. J. Best, Anthropogenic stresses on the world's big rivers. *Nat. Geosci.* **12**, 7–21 (2019).
22. D. A. Sánchez-Núñez, J. E. Mancera Pineda, A. F. Osorio, From local-to global-scale control factors of wave attenuation in mangrove environments and the role of indirect mangrove wave attenuation. *Estuarine, Coastal Shelf Sci.* **245**, 106926 (2020).
23. H. Cao, Y. Chen, Y. Tian, W. Feng, Field Investigation into wave attenuation in the mangrove environment of the South China Sea Coast. *J. Coastal Res.* **32**, 1417–1427 (2016).
24. Y. Mazda, M. Magi, Y. Ikeda, T. Kurokawa, T. Asano, Wave reduction in a mangrove forest dominated by *Sonneratia* sp. *Wetlands Ecol. Manage.* **14**, 365–378 (2006).
25. X. Zhou, Z. Dai, W. Pang, J. Wang, C. Long, Wave attenuation over mangroves in the Nanliu Delta, China. *Front. Mar. Sci.* **9**, 874818 (2022).
26. S. Quartel, A. Kroon, P. G. E. F. Augustinus, P. Van Santen, N. H. Tri, Wave attenuation in coastal mangroves in the Red River Delta, Vietnam. *J. Asian Earth Sci.* **29**, 576–584 (2007).
27. V. L. H. Phuoc, S. R. Massel, Experiments on wave motion and suspended sediment concentration at Nang Hai, Can Gio mangrove forest, Southern Vietnam. *Oceanologia* **48**, 23–40 (2006).
28. E. M. Horstman *et al.*, Wave attenuation in mangroves: A quantitative approach to field observations. *Coastal Eng.* **94**, 47–62 (2014).
29. C. A. Vanegas, A. F. Osorio, L. E. Urrego, Wave dissipation across a Rhizophora mangrove patch on a Colombian Caribbean Island: An experimental approach. *Ecol. Eng.* **130**, 271–281 (2019).
30. A. Achim, B. C. Nicoll, Modelling the anchorage of shallow-rooted trees. *Forestry* **82**, 273–284 (2009).
31. R. S. Jadhav, Q. Chen, J. M. Smith, Spectral distribution of wave energy dissipation by salt marsh vegetation. *Coastal Eng.* **77**, 99–107 (2013).
32. F. Ursell, The long-wave paradox in the theory of gravity waves. *Math. Proc. Cambridge Philos. Soc.* **49**, 685–694 (1953).
33. W.-C. Wu, D. T. Cox, Effects of wave steepness and relative water depth on wave attenuation by emergent vegetation. *Estuarine, Coastal Shelf Sci.* **164**, 443–450 (2015).
34. K. L. Phan, M. J. F. Stive, M. Zijlema, H. S. Truong, S. G. J. Aarninkhof, The effects of wave non-linearity on wave attenuation by vegetation. *Coastal Eng.* **147**, 63–74 (2019).
35. T. J. Bouma *et al.*, Trade-offs related to ecosystem engineering: A case study on stiffness of emerging macrophytes. *Ecology* **86**, 2187–2199 (2005).
36. R. van Hespen *et al.*, Analysis of coastal storm damage resistance in successional mangrove species. *Limnol. Oceanogr.* **66**, 3221–3236 (2021), 10.1002/lno.11875.
37. A. Etminan, R. J. Lowe, M. Ghisalberti, Canopy resistance on oscillatory flows. *Coastal Eng.* **152**, 103502 (2019).
38. Z. Hu *et al.*, Laboratory data on wave propagation through vegetation with following and opposing currents. *Earth Syst. Sci. Data* **13**, 4987–4999 (2021).
39. M. Maza, J. L. Lara, I. J. Losada, A paradigm shift in the quantification of wave energy attenuation due to saltmarshes based on their standing biomass. *Sci. Rep.* **12**, 13883 (2022).
40. X. Wang *et al.*, Rebound in China's coastal wetlands following conservation and restoration. *Nat. Sustainability* **4**, 1076–1083 (2021).
41. N. Xu *et al.*, Effects of waves, burial depth and material density on microplastic retention in coastal sediments. *Sci. Total Environ.* **864**, 161093 (2023).
42. M. J. Tucker, E. G. Pitt, *Waves in Ocean Engineering* (Elsevier Science, ed. 1, 2001).
43. M. Zijlema, G. Stelling, P. Smit, SWASH: An operational public domain code for simulating wave fields and rapidly varied flows in coastal waters. *Coastal Eng.* **58**, 992–1012 (2011).
44. J. R. Morison, J. W. Johnson, S. A. Schaaf, The force exerted by surface waves on piles. *J. Pet. Technol.* **2**, 149–154 (1950).
45. Z. Hu *et al.*, Data processing code of the HU method to assess wave dissipation capacity of coastal and estuarine forested wetlands. 4TU.ResearchData. https://doi.org/10.4121/bbb3cf31-043a-40a4-9bbc-42c599874db3.v5. Accessed 12 February 2025.

Downloaded from https://www.pnas.org by 84.17.46.190 on April 30, 2025 from IP address 84.17.46.190.